Methods 151 (2018) 21–27

Contents lists available at ScienceDirect

Methods

journal homepage: www.elsevier.com/locate/ymeth

Tumor classification with MALDI-MSI data of tissue microarrays: A case study

Nadine E. Mascini[a], Jannis Teunissen[b,c], Rob Noorlag[d], Stefan M. Willems[e], Ron M.A. Heeren[f,a,*]

[a] AMOLF, Science Park 104, 1098 XG Amsterdam, The Netherlands
[b] Centrum Wiskunde en Informatica (CWI), P.O. Box 94079, 1090 GB Amsterdam, The Netherlands
[c] Centre for Mathematical Plasma Astrophysics, Department of Mathematics, KU Leuven, Celestijnenlaan 200B, B-3001 Leuven, Belgium
[d] Department of Oral and Maxillofacial Surgery, University Medical Center Utrecht, Heidelberglaan 100, 3584 CX Utrecht, The Netherlands
[e] Department of Pathology, University Medical Center Utrecht, Heidelberglaan 100, 3584 CX Utrecht, The Netherlands
[f] The Maastricht MultiModal Molecular Imaging Institute (M4I), Maastricht University, Universiteitssingel 50, 6229 ER Maastricht, The Netherlands

ARTICLE INFO

Keywords:
Mass spectrometry imaging
MALDI
Tissue microarray
FFPE tissue
Head and neck cancer
Data analytics

ABSTRACT

With mass spectrometry imaging (MSI) on tissue microarrays (TMAs) a large number of biomolecules can be studied for many patients at the same time, making it an attractive tool for biomarker discovery. Here we investigate whether lymph node metastasis can be predicted from MALDI-MSI data. Measurements are performed on TMAs and then filtered based on spectral intensity and the percentage of tumor cells, after which the resulting data for 122 patients is further preprocessed. We assume differences between patients with and without metastasis are expressed in a limited number of features. Two univariate feature selection methods are applied to reduce the dimensionality of the MALDI-MSI data. The selected features are then used in combination with three classifiers. The best classification scores are obtained with a decision tree classifier, which classifies about 72% of patients correctly. Almost all the predictive power comes from a single peak (m/z 718.4). The sensitivity of our classification approach, which can be generically used to search for biomarkers, is investigated using artificially modified data.

1. Introduction

With matrix-assisted laser desorption/ionization mass spectrometry imaging (MALDI-MSI), biomolecules such as proteins, peptides, lipids and metabolites can be studied directly from tissue sections. Up to thousands of biomolecular species can be studied simultaneously and tissues with different disease states can be compared to find differences in the expression of biomolecules. In this way, biomarkers or biomarker patterns might be identified that are associated with specific disease states.

Tissue microarray (TMA) samples consist of arrays of small tissue pieces from different patients. Using TMAs, one can measure a large sample set under highly similar experimental conditions, and correlate the acquired data with clinical data. These properties make TMAs well suited for biomarker discovery studies. Up to a thousand patient samples per study can now be analyzed in a MALDI-MSI experiment [1].

There have been several studies that correlate MALDI-MSI data with cancer progression, see for example [2–8]. So far, many studies that were successful in the identification of prognostic markers performed intact protein analysis on fresh frozen tissue sections [3,8]. In [1,9,10] TMAs with samples from more than 100 patients were used. An important step in MALDI-MSI classification studies is to select features out of the high-dimensional data. This can for example be done based on the score of a univariate statistical test, or by performing Principal Component Analysis (PCA) and keeping only a few principal components. There are several ways to investigate the predictive power of the selected features. Perhaps the simplest way is to correlate individual features to the parameter of interest [1,9]. It is also possible to combine features to increase their predictive power, for example by Hierarchical Clustering [3,5,8]. Alternatively, a classifier can be trained to predict the parameter of interest from the features [3,7,11]. Regardless of the approach chosen, the number of features associated with a prognostic parameter is typically less than 20. In some studies, an independent validation of the identified proteins is provided by immunohistochemistry.

Head and neck cancer is the world's sixth most common cancer. Despite advances in diagnostics and treatment strategies, survival rates have not improved over the last decades and remain poor, with a 5-year survival of approximately 50% [12]. The presence of lymph node metastasis at the time of diagnosis is a major predictor for prognosis.

* Corresponding author at: The Maastricht MultiModal Molecular Imaging Institute (M4I), Maastricht University, Universiteitssingel 50, 6229 ER Maastricht, The Netherlands.
E-mail address: r.heeren@maastrichtuniversity.nl (R.M.A. Heeren).

https://doi.org/10.1016/j.ymeth.2018.04.004
Received 3 November 2017; Received in revised form 4 March 2018; Accepted 9 April 2018
Available online 12 April 2018

Unfortunately, in around 30% of patients existing lymph node metastases are not detected with current diagnostic imaging techniques such as ultrasound-guided fine needle aspiration cytology (FNAC), computed tomography (CT) and magnetic resonance imaging (MRI).

Tumor profiling with biomarkers has recently shown promising results [13,14]. A validated gene expression profile accurately predicted the absence of nodal metastasis in 89% of the patients. However, the use of this gene profile would lead to a large number of patients undergoing unnecessary treatment [15]. Mass-spectrometry based proteomic methods have been applied to identify markers associated with tumor aggressiveness and metastasis in oral cancer. Polachini et al. found 155 differentially expressed proteins favoring metastasis [16]. More recently, a proteomic analysis by Harris et al. revealed 72 peptide features associated with disease-specific death, metastasis and recurrence [17]. However, to our knowledge no proteomic profile with predictive capability has been generated yet.

This work focuses on the processing and analysis of high-dimensional MALDI-MSI data from TMAs to find biomarkers for head and neck cancer. We describe the quality measures taken to avoid the introduction of bias during data generation and data analysis, and we assess the sensitivity of our classification approach. Finally, we test whether we can predict lymph node metastasis from MALDI-MSI data of head and neck cancer tumors.

2. Materials and methods

2.1. Patient samples

For this study, 240 patient samples were available: 212 cases of oral squamous cell carcinoma (OSCC) and 28 cases of oropharyngeal squamous cell carcinoma (OPSCC). These samples came from patients with histologically proven oral or oropharyngeal squamous cell carcinoma that underwent surgery between 1996 and 2005 at the University Medical Center Utrecht in The Netherlands. Patients diagnosed with synchronous primary tumors or previous malignancies in the head and neck region were not included in this cohort [18].

In our study, we use two TMAs that contain tissue cores excised from 120 patient samples. Per patient, three cores (0.6 mm in diameter) of the central part of the primary tumor were present, see Fig. 1b. In Table 1, the number of patients which showed lymph node metastasis is listed. The two classes were randomly distributed across the TMAs. It is important to have a random distribution of the samples across a TMA to ensure the location of the samples on the TMA(s) is not a confounding factor in the analysis.

Table 1
The patient samples used in this study.

Class description	Yes	No
Lymph node metastasis	134	106

2.2. Sample preparation

The TMAs contain formalin-fixed paraffin-embedded (FFPE) tissue. This tissue is conserved by dehydration and cross-linking of the proteins with formalin. After formalin fixation, the tissue is embedded in paraffin to preserve tissue morphology and allow thin sectioning of the tissue. FFPE tissue is widely used for clinical applications, due to easy storage and handling.

The TMAs were prepared for MALDI-MSI analysis as previously described in [19]. We summarize the important steps below. First, serial 5 µm tick tissue sections were cut from the TMA blocks and mounted onto conductive indium tin oxide (ITO) coated glass slides (Delta Technologies, USA). Paraffin was removed using xylene washes (twice, 5 min). Paraffin needs to be removed, as it causes ion suppression during mass spectrometric analysis.

The goal of the next steps in the sample preparation is to make the proteins amenable to MSI analysis. First, rehydration is performed using graded ethanol washes (100%, 100%, 95%, 75% and 30%, all 5 min) and water washes (twice, 3 min). The used solvents were HPLC-grade. Then, (part of) the cross-linking is reversed (most likely through heat-induced hydrolysis [20]) by incubation of the sample in a buffer at high temperature. The samples were incubated at 95 °C in a 10 mM Tris buffer pH 9 for 20 min, and allowed to cool down to room temperature before briefly rinsing them with water. Afterwards, the samples were dried in a desiccator.

Trypsin was dissolved in 50 mM ammoniumbicarbonate plus 25 µM octylglucoside at a final concentration of 0.05 µg/µL. On-tissue digestion was performed using a Suncollect automatic sprayer (SunChrom, Germany). Eight layers were applied with a flow rate of 7.5 µL/min. The quick movement of the localized spray over the tissue ensures that the spatial information is retained. The samples were incubated at 37 °C overnight in a humid environment (50% methanol in deionized water).

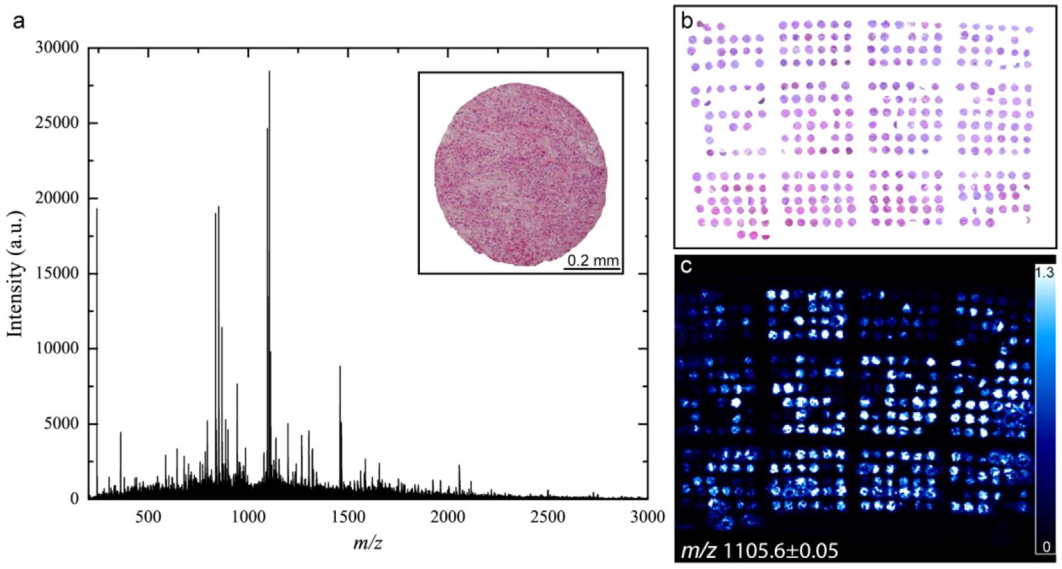

Fig. 1. Example of a head and neck cancer TMA. (a) Unprocessed MALDI-MSI spectrum from a tissue core. Inset: Hematoxylin and eosin (H&E) stained tissue core with 80% tumor cells. (b) H&E stained TMA of 120 patients. (c) Selected ion image shows the distribution of a typical peptide peak.

Proteins in FFPE tissue are typically digested with trypsin to free them from remaining cross-links and aggregation which hinder their detection.

A matrix solution of 5 mg/mL alpha-cyano-4-hydroxycinnamic acid (CHCA) in 1:1 ACN:H_2O with 0.1% trifluoroacetic acid was used. Matrix was applied with the Suncollect sprayer. Eight successive coats were applied with an increasing flow rate of 7.5–20 μL/min.

2.3. MALDI-MSI measurements

The experiments were performed with a MALDI-QTOF instrument (Synapt G2Si HDMS, Waters, UK) in positive mode and an m/z range of 200–3500. Spectra were acquired with a stage step size of 100 μm and a laser frequency of 1000 Hz (laser spot diameter 60 μm), with the quadrupole set to have optimal transmission in the peptide region of the mass spectrum. The instrument was operated in sensitivity mode during all experiments, and on average 34 spatially resolved spectra were recorded for each core. Two data sets were acquired for each TMA; the second set of samples was rotated 180 degrees during preparation and measurement to avoid the introduction of bias.

MALDI-MSI spectra of FFPE tissue consist mainly of tryptic peptide and matrix peaks. An exemplary unprocessed mass spectrum can be found in Fig. 1a. MALDI-MSI studies of TMAs report the detection of around 500 peptide peaks [21,22]. This is in line with our observation of on average 700 tissue-related peaks per patient in the range of m/z 700–3500.

As was previously observed for FFPE tissue [23], the baseline of the spectrum has a hill shape. This feature becomes more pronounced after peak-picking of the spectra, see the next section and Fig. 2. The elevated baseline is most likely caused by the rich mixture of molecules that is desorbed and ionized from the digested tissue surface. Formalin fixation-induced adducts might further increase the number of different ionized species [24]. Unresolved peaks lead to a loss in spectral resolution and a decrease in signal-to-noise ratio. A shorter digestion time of two hours did not improve the quality of the spectra. Replacing the Tris buffer (pH 9) with an acidic buffer (10 mM citric acid at pH 6), as was used in [25], did also not improve the signal-to-noise ratio.

2.4. Tissue core selection and pre-processing of the spectra

After MALDI-MSI analysis, the samples were washed with 100% MeOH to remove the matrix and stained with hematoxylin and eosin (H&E) using a standard protocol, see Fig. 1b. The percentage of tumor cells per tissue core was determined by a dedicated head and neck pathologist. Only tissue cores with more than 80% tumor cells were used in this study. After this procedure there were still spectra from 122 patients, of which 74 were lymph node metastasis positive and 48 lymph node metastasis negative. Clinical follow-up data were available for all 122 patients (Supplementary Information).

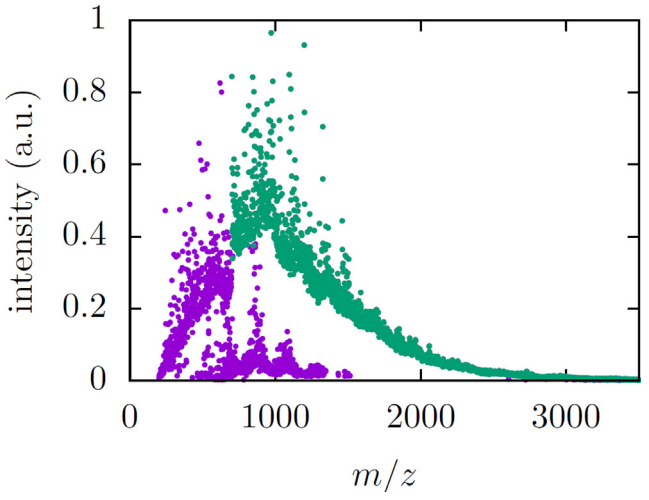

Fig. 2. Example of a peak-picked spectrum, obtained by combining data from all tumor cores of the same patient. The m/z values indicated by purple dots are filtered out during the pre-processing. (For interpretation of the references to colour in this figure legend, the reader is referred to the web version of this article.)

Spectra from the cores were extracted for data processing and subsequent statistical analysis using an in-house developed MATLAB-based software tool (The Mathworks, USA). This tool co-registers the MSI data and the H&E scan of the same sample to accurately extract 'on-tissue' spectra. The extracted spectra were subjected to peak detection using the PEAPI algorithm [26].

Two data sets were acquired for each TMA; the second set of samples was rotated 180 degrees during preparation and measurement to avoid the introduction of bias.

We tested the introduction of bias due to the location of the tissue cores on the tissue microarray slides by measuring serial sections which were rotated 180 degrees relative to the others during preparation and measurement. We could not detect a significant influence of the location on the data.

2.5. Data processing

For each patient, we have performed measurements on all available tumor cores (maximum three), and for each core, spectra were obtained at multiple locations or *pixels*. To reduce the variance in these measurements, they are combined per patient by summation. Afterwards, matrix-related peaks are removed, as illustrated by the purple dots in Fig. 2. All peaks below $m/z = 700$ are filtered out, because most of them do not correspond to peptides. In the region of m/z 700–1500 peaks related to the matrix are located at the bottom of the spectrum, see Fig. 2. To remove these peaks, the average patient spectrum is first smoothed with a second order Savitzky-Golay filter, and then peaks that lie below 75% of the smoothed average are removed. This Savitzky-Golay filter has a width of 125 data points, corresponding to an m/z range of 125. We then compute the average spectrum of all patients and its baseline, again using a second order Savitzky-Golay filter with a width of 125 data points. Note that 125 data points can now correspond to a larger m/z range because some peaks have been removed. Peaks that on average lie below the baseline are then removed from all patient spectra.

Since the patient spectra have slightly different baselines, we perform baseline correction per patient. For each patient, we first estimate the baseline with a median filter over a width of 125 data points. This estimate of the baseline is still rather noisy, so we smooth it with a second order Savitzky-Golay filter of the same width. For each patient, the smoothed baseline is then subtracted from the data, as illustrated in Fig. 3a. It is possible that some of the peaks lie below the baseline, so that they have a negative intensity after this procedure. This poses no problem for our classification approach, however. Finally, the baseline-corrected spectra per patient are normalized by total intensity. Fig. 3b shows examples of the resulting spectra for three randomly selected patients between $m/z = 1000$ and $m/z = 1200$. The processed spectra are qualitatively quite similar, but note that some of the peaks show significant differences between patients, which cannot be corrected for through a single normalization constant.

We remark that it would often be better to perform per-patient baseline correction and normalization before further data processing. However, the procedure described above, in which matrix and low-intensity peaks are first removed, gave us better qualitative agreement between patient spectra.

2.6. Feature selection

There are several ways to select features (i.e. m/z values), see for

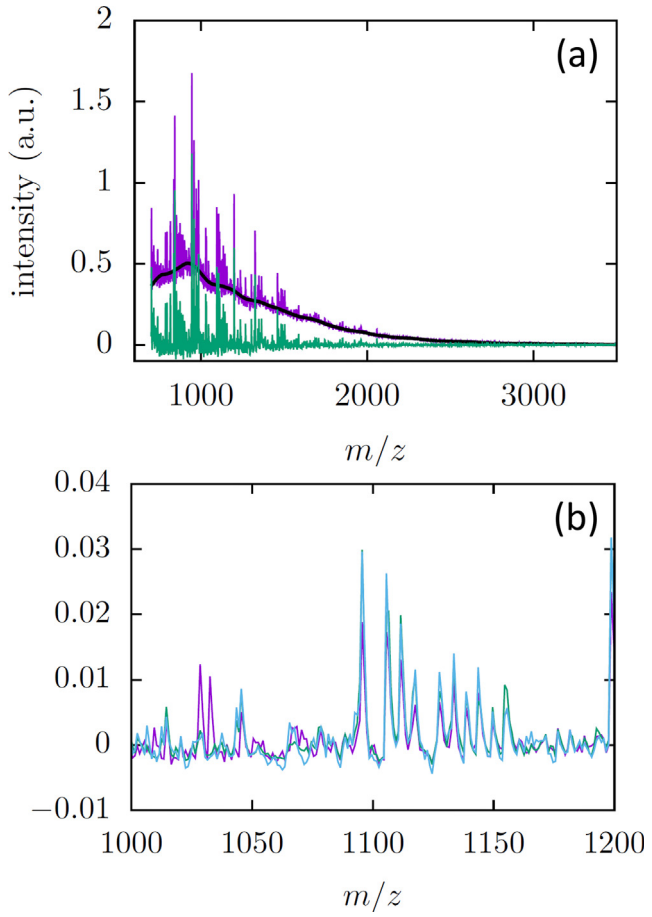

Fig. 3. (a) Example of a peak-picked spectrum with its baseline (black solid curve). The spectrum after baseline subtraction is also shown (green spectrum). (b) Examples of peak-picked spectra of three patients, after pre-processing, zoomed in on the range m/z 1000–1200. Peak-picked spectra are shown as continuous graphs for better readability. (For interpretation of the references to colour in this figure legend, the reader is referred to the web version of this article.)

example the discussion by Hilario et al. in Ref. [27]. Here we use univariate feature selection, which means that the features are ranked individually. We assume that class differences are expressed in a limited number of features, for example no more than five or ten. Individual features are then likely to show significant univariate differences. After several features have been selected by a univariate approach, a suitable classifier can combine them, potentially in a complex way.

We use two univariate statistical tests: the Wilcoxon rank-sum test and the Kolmogorov-Smirnov test. These tests are performed on our training data, which contains two classes, to estimate how (dis)similar peaks are distributed in these classes. To select N features, the N peaks with the smallest p-values are retained.

2.7. Classification

Different types of classifiers have their own strengths and weaknesses, depending on the data that they are applied to. Since we do not know a priori what types of patterns will be present in our data, we use three different classifiers, as implemented in the Scikit-Learn library [28]:

- LDA: Linear Discriminant Analysis, which works well for linearly separable data.
- NBC: Naive Bayes Classifier, which can work well for data in which each single feature independently has (some) predictive power.
- DTC: Decision Tree Classifier, with a maximum depth of three. This classifier can handle more complex relations between the features by construction of a 'decision tree'.

To test the performance of the different classifiers, we use so-called k-fold cross-validation, with $k = 10$. The data is randomly partitioned into 10 subsamples of nearly equal size. Each subsample is once used for testing, with the rest of the data used for feature selection and training. Data from a patient is thus either used for testing or for training, but never for both. After cross-validation, each patient has been part of the test-group exactly once, so a full set of predicted class labels is obtained. Then the number of true positives (*TP*), true negatives (*TN*), false positives (*FP*) and false negatives (*FN*) is determined.

3. Results and discussion

3.1. Classification of lymph node metastasis

The performance of binary classifiers can be judged by different metrics. Here we use a measure that can also be used when classes are of unequal size, namely Matthews correlation coefficient (MCC), also known as the φ coefficient:

$$MCC = \frac{TPxTN - FPxFN}{\sqrt{(TP + FP)(TP + FN)(TN + FP)(TN + FN)}}$$

,where TP is the number of true positives etc. The MCC coefficient lies between −1 and 1; these values indicate all predictions are wrong or correct, respectively, whereas 0 indicates there is no predictive power. If there are for example two equal size classes, for both of which 75% of the predictions is correct, the MCC score is 0.5.

The prediction of lymph node metastasis using our workflow is shown in Fig. 4. For Fig. 4a these features were selected using the Wilcoxon rank-sum tests. The best results are obtained the decision tree classifier in combination with one or two features, by far the most important of which is $m/z = 718.4$. This results in an MCC score of about 0.4, and about 72% of the patients being classified correctly (TP, FP, TN, FN = 59 19 29 15). For reference, this corresponds to a sensitivity of 80% and a specificity of 60%. This classification accuracy is comparable to the results of [15] (72% negative predictive value), which used a gene signature to predict lymph node metastasis.

For Fig. 4b the Kolmogorov-Smirnov test was used, and in combination with the decision tree classifier we also observe MCC scores of up to about 0.4 and 72% correct classifications. The same tissue-derived ion ($m/z = 718.4$) is again responsible for almost all the predictive power. The significance of a result is often expressed by the number of standard deviations it corresponds to. As discussed below and shown in Fig. 5, the standard deviation in the MCC scores is about 0.15 when using randomized class labels, so that a score of 0.4 corresponds to almost three standard deviations. In Fig. 6 samples from the two metastasis classes are visualized using the $m/z = 718.4$ feature. The patients with and without metastasis have a different distribution, although there is also considerable overlap. MS/MS experiments might be performed to identify the tissue-derived ion at m/z 718.4.

3.2. Sensitivity of method

To get an idea of the sensitivity of the classification approach, we have performed tests with modified data. First, one representative peak with an m/z value of 1325.7 was selected, which had an average intensity. Then the class labels were randomized, after which the m/z 1325.7 peak was increased with a certain percentage in one of the classes. This increase was performed *after pre-processing*, but before feature selection. Then five features were selected using the Kolmogorov-Smirnov test, after which the LDA classifier was applied (we could also have used the naive Bayes or the decision tree classifier,

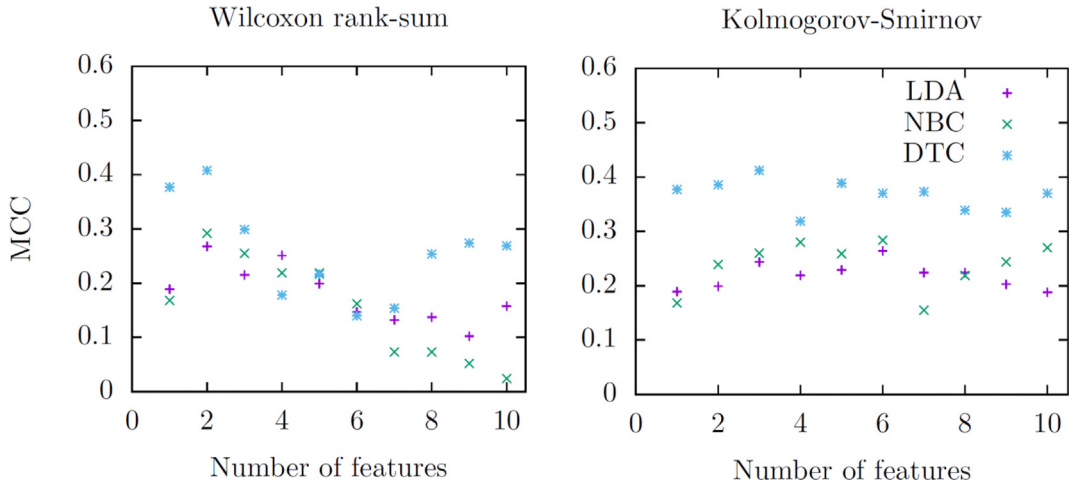

Fig. 4. Classification results for lymph node metastasis (a, b). The left figures show results for feature selection with the Wilcoxon rank-sum test. The right figures show results using the Kolmogorov-Smirnov test.

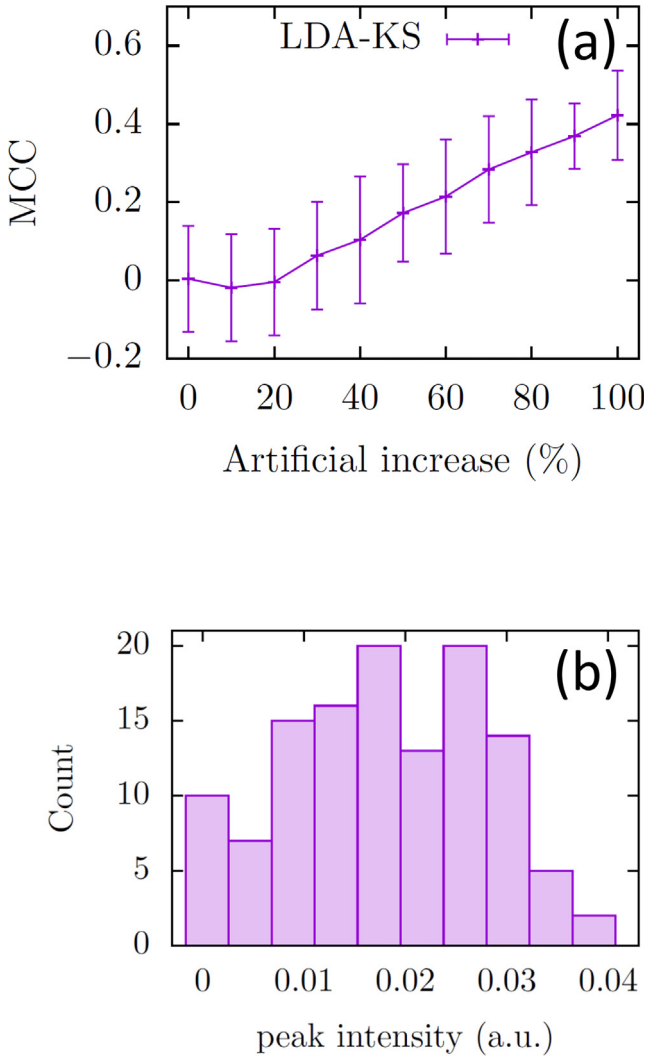

Fig. 5. (a) Test of the Kolmogorov-Smirnov feature selection method using *artificial* data. A typical peptide peak at m/z 1325.7 has been increased by a certain percentage in one of the classes. The error bars indicate plus and minus one standard deviation. Data was collected from 40 runs with randomized class labels. (b) Histogram of the peptide peak at m/z 1325.7 after preprocessing.

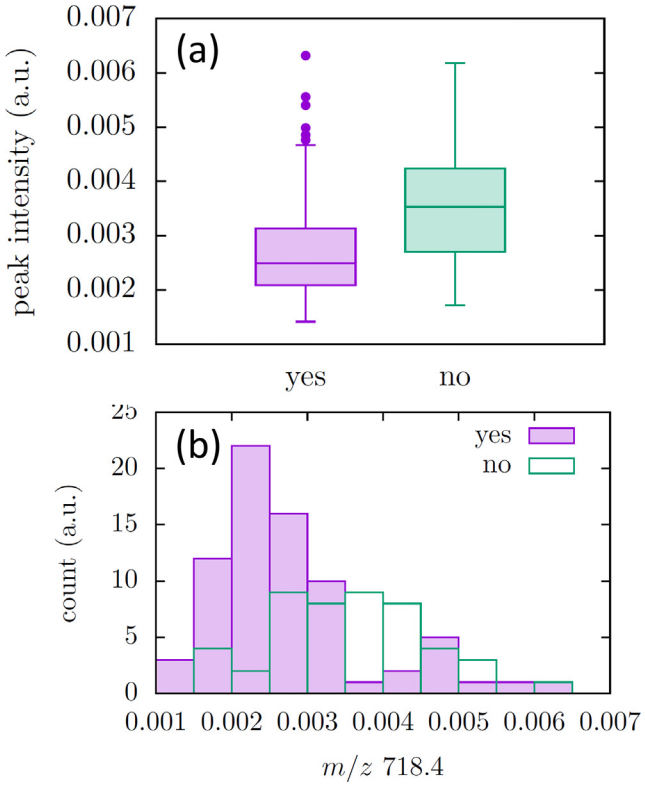

Fig. 6. (a) Box plot (whiskers at 1.5 times the interquartile range, with outliers indicated) of the m/z 718.4 peak for patients with and without metastasis. (b) A histogram of the m/z 718.4 peak for patients with and without metastasis.

all work well for this type of artificial difference). Classification results for different increases are shown in Fig. 5a, based on data from 40 runs with randomized class labels. The error bars indicate the standard deviations in the MCC score, which are about 0.15. With an artificial increase of 70%, the MCC score is about 0.3, which corresponds to two standard deviations. Using the method and data presented here, we can thus expect significant classification scores when the intensity of a single peak differs by 70% between the classes. When multiple peaks would show a similar increase, classification scores would drastically go up, as long as the univariate differences are large enough for our feature selection procedure. We remark that the above results with modified data strongly depend on the signal to noise ratio of the spectra. When

this ratio is high, peak intensities are large compared to their typical fluctuations, making it easier to distinguish class differences from random noise.

3.3. Tissue heterogeneity

A high signal to noise ratio of spectra and individual peaks is key for the successful detection of biomarkers. A challenge in this regard is that head and neck cancer tissue is quite heterogeneous: a small piece of a single tumor may contain different types of tissue. MALDI-MSI can help to overcome this, because it allows for histology-directed analysis. The approach taken here was to include tissue cores based on their tumor cell percentage, as determined by a dedicated head and neck pathologist. This was done because we use relatively small cores with a diameter of 0.6 mm. In studies with larger tissue cores it is also possible to select regions within a core, as done for example by Buck et al. for metabolite imaging [29].

For the results presented in this paper we used tissue cores containing at least 80% tumor cells. When we instead select tumors cores containing at least 50% tumor cells, classification scores go drastically down. The *m/z* 718.4 peak is still selected in the majority of cases, but the best MCC scores are now below 0.1; much lower than the score of 0.4 found when using 80% tumor cells.

4. Conclusions

We have used MALDI-MSI data from head and neck cancer TMAs for the purpose of biomarker prediction. A large and well-matched set of tumors was used, which helps to compensate for the intrinsic heterogeneity of patient samples. The experimental methodology and the preprocessing of the obtained spectra was described, as well as the construction of a classifier for lymph node metastasis. We used two univariate feature selection methods, three different classifiers, and between one and ten features. The best results were obtained with a decision tree classifier, and almost all the predictive power was based on a single peak (*m/z* 718.4). We also demonstrated the sensitivity of our classification method, using artificially modified data.

The primary assumption behind our approach is that class differences are expressed in a limited number of features/peaks, so that they can be selected with a univariate test. Our approach is then a relatively simple way to search for biomarkers in MALDI-MSI data. Afterwards, independent validation of the found markers or patterns can be performed with different samples and different analytical methods.

Acknowledgements

Part of this work belongs to the research programme of the Netherlands Organisation for Scientific Research (NWO) and was performed at the research institute AMOLF. RH acknowledges financial support of the LINK program of the Dutch Province of Limburg. NM and RH acknowledge financial support from the Dutch national program COMMIT. RN acknowledges financial support from the Dutch Cancer Society (research grant: 2014-6620). The authors thank Dr. Robert van Es and the department of Head and Neck Surgical Oncology for providing the clinical data.

Appendix A. Supplementary data

Supplementary data associated with this article can be found, in the online version, at http://dx.doi.org/10.1016/j.ymeth.2018.04.004.

References

[1] S. Steurer, C. Borkowski, S. Odinga, M. Buchholz, C. Koop, H. Huland, M. Becker, M. Witt, D. Trede, M. Omidi, O. Kraus, A.S. Bahar, A.S. Seddiqi, J.M. Singer, M. Kwiatkowski, M. Trusch, R. Simon, M. Wurlitzer, S. Minner, T. Schlomm, G. Sauter, H. Schlüter, MALDI mass spectrometric imaging based identification of clinically relevant signals in prostate cancer using large-scale tissue microarrays, Int. J. Cancer. 133 (2013) 920–928, http://dx.doi.org/10.1002/ijc.28080.

[2] W.M. Hardesty, M.C. Kelley, D. Mi, R.L. Low, R.M. Caprioli, Protein signatures for survival and recurrence in metastatic melanoma, J. Proteomics 74 (2011) 1002–1014, http://dx.doi.org/10.1016/j.jprot.2011.04.013.

[3] B. Balluff, S. Rauser, S. Meding, M. Elsner, C. Schöne, A. Feuchtinger, C. Schuhmacher, A. Novotny, U. Jtting, G. MacCarrone, H. Sarioglu, M. Ueffing, H. Braselmann, H. Zitzelsberger, R.M. Schmid, H. Höfler, M.P. Ebert, A. Walch, MALDI imaging identifies prognostic seven-protein signature of novel tissue markers in intestinal-type gastric cancer, Am. J. Pathol. 179 (2011) 2720–2729, http://dx.doi.org/10.1016/j.ajpath.2011.08.032.

[4] S. Meding, B. Balluff, M. Elsner, C. Schöne, S. Rauser, U. Nitsche, M. Maak, A. Schäfer, S.M. Hauck, M. Ueffing, R. Langer, H. Höfler, H. Friess, R. Rosenberg, A. Walch, Tissue-based proteomics reveals FXYD3, S100A11 and GSTM3 as novel markers for regional lymph node metastasis in colon cancer, J. Pathol. 228 (2012) 459–470, http://dx.doi.org/10.1002/path.4021.

[5] M. Nipp, M. Elsner, B. Balluff, S. Meding, H. Sarioglu, M. Ueffing, S. Rauser, K. Unger, H. Höfler, A. Walch, H. Zitzelsberger, S100–A10, thioredoxin, and S100–A6 as biomarkers of papillary thyroid carcinoma with lymph node metastasis identified by MALDI Imaging, J. Mol. Med. 90 (2012) 163–174, http://dx.doi.org/10.1007/s00109-011-0815-6.

[6] K. Yanagisawa, Y. Shyr, B.J. Xu, P.P. Massion, P.H. Larsen, B.C. White, J.R. Roberts, M. Edgerton, A. Gonzalez, S. Nadaf, J.H. Moore, R.M. Caprioli, D.P. Carbone, Proteomic patterns of tumour subsets in non-small-cell lung cancer, Lancet (London, England) 362 (2003) 433–439, http://dx.doi.org/10.1016/S0140-6736(03)14068-8.

[7] S.A. Schwartz, R.J. Weil, R.C. Thompson, Y. Shyr, J.H. Moore, S.A. Toms, M.D. Johnson, R.M. Caprioli, Proteomic-based prognosis of brain tumor patients using direct-tissue matrix-assisted laser desorption ionization mass spectrometry, Cancer Res. 65 (2005) 7674–7681, http://dx.doi.org/10.1158/0008-5472.CAN-04-3016.

[8] M. Elsner, S. Rauser, S. Maier, C. Schöne, B. Balluff, S. Meding, G. Jung, M. Nipp, H. Sarioglu, G. Maccarrone, M. Aichler, A. Feuchtinger, R. Langer, U. Jütting, M. Feith, B. Küster, M. Ueffing, H. Zitzelsberger, H. Höfler, A. Walch, MALDI imaging mass spectrometry reveals COX7A2, TAGLN2 and S100–A10 as novel prognostic markers in Barrett's adenocarcinoma, J. Proteomics 75 (2012) 4693–4704, http://dx.doi.org/10.1016/j.jprot.2012.02.012.

[9] A. Quaas, A.S. Bahar, K. von Loga, A.S. Seddiqi, J.M. Singer, M. Omidi, O. Kraus, M. Kwiatkowski, M. Trusch, S. Minner, E. Burandt, P. Stahl, W. Wilczak, M. Wurlitzer, R. Simon, G. Sauter, A. Marx, H. Schlüter, MALDI imaging on large-scale tissue microarrays identifies molecular features associated with tumour phenotype in oesophageal cancer, Histopathology 63 (2013) 455–462, http://dx.doi.org/10.1111/his.12193.

[10] A. Hinsch, M. Buchholz, S. Odinga, C. Borkowski, C. Koop, J.R. Izbicki, M. Wurlitzer, T. Krech, W. Wilczak, S. Steurer, F. Jacobsen, E.C. Burandt, P. Stahl, R. Simon, G. Sauter, H. Schl??ter, MALDI imaging mass spectrometry reveals multiple clinically relevant masses in colorectal cancer using large-scale tissue microarrays, J. Mass Spectrom. 52 (2017) 165–173, http://dx.doi.org/10.1002/jms.3916.

[11] S. Meding, U. Nitsche, B. Balluff, M. Elsner, S. Rauser, C. Schöne, M. Nipp, M. Maak, M. Feith, M.P. Ebert, H. Friess, R. Langer, H. Höfler, H. Zitzelsberger, R. Rosenberg, A. Walch, Tumor classification of six common cancer types based on proteomic profiling by MALDI imaging, J. Proteome Res. 11 (2012) 1996–2003, http://dx.doi.org/10.1021/pr200784p.

[12] A. Jemal, F. Bray, M.M. Center, J. Ferlay, E. Ward, D. Forman, Global cancer statistics, CA Cancer J. Clin. 61 (2011) 69–90, http://dx.doi.org/10.3322/caac.20107.

[13] R. de Bree, R.P. Takes, J.A. Castelijns, J.E. Medina, S.J. Stoeckli, A.A. Mancuso, J.L. Hunt, J.P. Rodrigo, A. Triantafyllou, A. Teymoortash, F.J. Civantos, A. Rinaldo, K.T. Pitman, M. Hamoir, K.T. Robbins, C.E. Silver, O.S. Hoekstra, A. Ferlito, Advances in diagnostic modalities to detect occult lymph node metastases in head and neck squamous cell carcinoma, Head Neck 37 (2015) 1829–1839, http://dx.doi.org/10.1002/hed.23814.

[14] A. Teymoortash, S. Hoch, B. Eivazi, J.A. Werner, Postoperative morbidity after different types of selective neck dissection, Laryngoscope 120 (2010), http://dx.doi.org/10.1002/lary.20894.

[15] S.R. Van Hooff, F.K.J. Leusink, P. Roepman, R.J. Baatenburg De Jong, E.J.M. Speel, M.W.M. Van Den Brekel, M.L.F. Van Velthuysen, P.J. Van Diest, R.J.J. Van Es, M.A.W. Merkx, J.A. Kummer, C.R. Leemans, E. Schuuring, J.A. Langendijk, M. Lacko, M.J. De Herdt, J.C. Jansen, R.H. Brakenhoff, P.J. Slootweg, R.P. Takes, F.C.P. Holstege, Validation of a gene expression signature for assessment of lymph node metastasis in oral squamous cell carcinoma, J. Clin. Oncol. 30 (2012) 4104–4110, http://dx.doi.org/10.1200/JCO.2011.40.4509.

[16] G.M. Polachini, L.M. Sobral, A.M.C. Mercante, A.F. Paes-Leme, F.C.A. Xavier, T. Henrique, D.M. Guimarães, A. Vidotto, E.E. Fukuyama, J.F. Góis-Filho, P.M. Cury, O.A. Curioni, P. Michaluart, A.M.A. Silva, V. Wünsch-Filho, F.D. Nunes, A.M. Leopoldino, E.H. Tajara, Proteomic approaches identify members of cofilin pathway involved in oral tumorigenesis, PLoS One 7 (2012) 1–13, http://dx.doi.org/10.1371/journal.pone.0050517.

[17] T.M. Harris, P. Du, N. Kawachi, T.J. Belbin, Y. Wang, N.F. Schlecht, T.J. Ow, C.E. Keller, G.J. Childs, R.V. Smith, R.H. Angeletti, M.B. Prystowsky, J. Lim, Proteomic analysis of oral cavity squamous cell carcinoma specimens identifies patient outcome-associated proteins, Arch. Pathol. Lab. Med. 139 (2015) 494–507, http://dx.doi.org/10.5858/arpa.2014-0131-OA.

[18] T.J.W. Klein Nulent, P.J. Van Diest, P. Van Der Groep, F.K.J. Leusink, C.L.J.J. Kruitwagen, R. Koole, E.M. Van Cann, Cannabinoid receptor-2

immunoreactivity is associated with survival in squamous cell carcinoma of the head and neck, Br. J. Oral Maxillofac. Surg. 51 (2013) 604–609, http://dx.doi.org/10.1016/j.bjoms.2013.03.015.
[19] R. Casadonte, R.M. Caprioli, Proteomic analysis of formalin-fixed paraffin-embedded tissue by MALDI imaging mass spectrometry, Nat. Protoc. 6 (2011) 1695–1709, http://dx.doi.org/10.1038/nprot.2011.388.
[20] S. Magdeldin, T. Yamamoto, Toward deciphering proteomes of formalin-fixed paraffin-embedded (FFPE) tissues, Proteomics. 12 (2012) 1045–1058, http://dx.doi.org/10.1002/pmic.201100550.
[21] M.-C. Djidja, E. Claude, M.F. Snel, S. Francese, P. Scriven, V. Carolan, M.R. Clench, Novel molecular tumour classification using MALDI-mass spectrometry imaging of tissue micro-array, Anal. Bioanal. Chem. 397 (2010) 587–601, http://dx.doi.org/10.1007/s00216-010-3554-6.
[22] T.M. Morgan, E.H. Seeley, O. Fadare, R.M. Caprioli, P.E. Clark, Imaging the clear cell renal cell carcinoma proteome, J. Urol. 189 (2013) 1097–1103, http://dx.doi.org/10.1016/j.juro.2012.09.074.
[23] R. Lemaire, A. Desmons, J.C. Tabet, R. Day, M. Salzet, I. Fournier, Direct analysis and MALDI imaging of formalin-fixed, Paraffin-Embedded Tissue Sections (2007), http://dx.doi.org/10.1021/PR060549I.
[24] Virginie Redeker, Jean-Yves Toullec, Joëlle Vinh, Jean Rossier, D. Soyez, Combination of peptide profiling by matrix-assisted laser desorption/ionization time-of-flight mass spectrometry and immunodetection on single glands or cells, Anal. Chem. (1998), http://dx.doi.org/10.1021/AC971309C.
[25] J.O.R. Gustafsson, M.K. Oehler, S.R. McColl, P. Hoffmann, Citric Acid Antigen Retrieval (CAAR) for tryptic peptide imaging directly on archived formalin-fixed paraffin-embedded tissue, J. Proteome Res. 9 (2010) 4315–4328, http://dx.doi.org/10.1021/pr9011766.
[26] G.B. Eijkel, B.K. Kaletaş, I.M. Van Der Wiel, J.M. Kros, T.M. Luider, R.M.A. Heeren, Correlating MALDI and SIMS imaging mass spectrometric datasets of biological tissue surfaces, Surf. Interface Anal. 41 (2009) 675–685, http://dx.doi.org/10.1002/sia.3088.
[27] M. Hilario, A. Kalousis, C. Pellegrini, M. Müller, Processing and classification of protein mass spectra, Mass Spectrom. Rev. 25 (2006) 409–449, http://dx.doi.org/10.1002/mas.20072.
[28] F. Pedregosa, G. Varoquaux, A. Gramfort, V. Michel, B. Thirion, O. Grisel, M. Blondel, P. Prettenhofer, R. Weiss, V. Dubourg, J. Vanderplas, A. Passos, D. Cournapeau, M. Brucher, M. Perrot, É. Duchesnay, Journal of machine learning research : JMLR., MIT Press, 2001. http://dl.acm.org/citation.cfm?id=2078195.
[29] A. Buck, B. Balluff, A. Voss, R. Langer, H. Zitzelsberger, M. Aichler, A. Walch, How suitable is matrix-assisted laser desorption/ionization-time-of-flight for metabolite imaging from clinical formalin-fixed and paraffin-embedded tissue samples in comparison to matrix-assisted laser desorption/ionization-fourier transform ion cyclotro, Anal. Chem. 88 (2016) 5281–5289, http://dx.doi.org/10.1021/acs.analchem.6b00460.